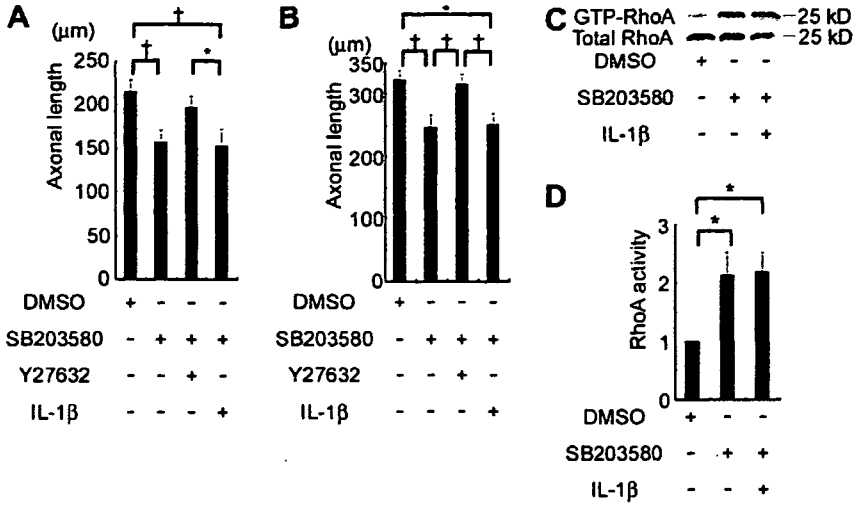

Fig. 4. IL-1β overcame neurite outgrowth inhibition via p38 MAPK pathway. (A and B) Axonal lengths were measured in DRG neuron culture (A) and CGN culture (B) using DMSO, SB203580, Y27632, or IL-1β. (C and D) Rho pull-down assay was performed (C) and intensities were measured (D). CGNs were cultured with DMSO, SB203580, or IL-1β for 15 min before lysed. Relative activities were quantified compared to the DMSO group. Error bars indicate the means ± SEM. $^{*}p < 0.05$ and $^{\dagger}p < 0.01$. Results are representative of three independent experiments.

tion of SB203580 increased RhoA activity to 2.1-fold compared with DMSO in CGNs (Fig. 4C and D). Moreover this was confirmed by the finding that Y27632 in addition to SB203580 increased axonal length (197.2 ± 18.2 μm in DRG neurons, 317.2 ± 16.1 μm in CGNs) compared with SB203580 (Fig. 4A and B). In contrast, IL-1β with SB203580 did not enhance axonal outgrowth (153.5 ± 10.5 μm in DRG neurons, 252.1 ± 13.8 μm in CGNs) and did not change RhoA activity (2.2-fold compared with DMSO) compared with SB203580 (Fig. 4A–D). These findings suggest that IL-1β overcame neurite outgrowth inhibition by deactivating RhoA via the p38 MAPK pathway. This is compatible with the previous report that IL-1β signal is mediated by p38 MAPK, and not by NF-κB in neurons [27]. Several studies using SB203580 or a dominant negative form of p38 MAPK indicate that p38 MAPK is essential for neurite outgrowth and growth cone formation [28,29]. p38 MAPK may thus be essential for nerve regeneration.

Sciatic nerve injury induces neuronal apoptosis in the spinal cord [30], and IL-1β may inhibit it as reported in retina [6]. During Wallerian degeneration, Schwann cells must proliferate to form bands of Büngner, and IL-1β may help this process [4]. These effects of IL-1β, promoting neuron survival, Schwann cell proliferation, and of course axonal elongation under myelin-derived inhibitory environment, help nerve regeneration. IL-1β is often considered a therapeutic target, due to its inflammatory effect, such as neutralizing antibody to IL-1β, interleukin-1 receptor antagonist, and inhibition of caspase-1, which converts pro-IL-1β into mature IL-1β [3]. On the other hand, beneficial effects have also been reported as noted above. Moreover, interleukin-1 receptor antagonist-releasing tubes delay sciatic nerve regeneration [31]. Thus, IL-1β is a "double-edged sword" with respect to nerve regeneration [32]. These opposing outcomes may be related to the degree and timing of inflammation. Since excess or untimely inflammation induces neuronal death, bringing about nerve degeneration [24], IL-1β may be useful as a therapeutic target. On the other hand, if inflammation is moderate and timely, it may aid nerve regeneration. It is thus important to control inflammation in appropriate degree and at the correct time, and IL-1β may play an essential role in this process in the nervous system.

Conclusion

Observations in the present study reveal that IL-1β overcomes neurite outgrowth inhibition by deactivating RhoA. Both p38 MAPK and NF-κB promote neurite outgrowth by inhibiting RhoA activity, and p38 MAPK, but not NF-κB, mediated IL-1β-induced neurite extension. Thus, IL-1β may contribute to nerve regeneration by overcoming MAG-induced neurite outgrowth inhibition after nerve injury.

References

[1] F.E. Perrin, S. Lacroix, M. Aviles-Trigueros, S. David, Involvement of monocyte chemoattractant protein-1, macrophage inflammatory protein-1alpha and interleukin-1beta in Wallerian degeneration, Brain 128 (2005) 854–866.

[2] S. Shamash, F. Reichert, S. Rotshenker, The cytokine network of Wallerian degeneration: tumor necrosis factor-alpha, interleukin-1alpha, and interleukin-1beta, J. Neurosci. 22 (2002) 3052–3060.

[3] A. Basu, J.K. Krady, S.W. Levison, Interleukin-1: a master regulator of neuroinflammation, J. Neurosci. Res. 78 (2004) 151–156.

[4] G. Conti, A. De Pol, E. Scarpini, F. Vaccina, M. De Riz, P. Baron, M. Tiriticco, G. Scarlato, Interleukin-1 beta and interferon-gamma induce proliferation and apoptosis in cultured Schwann cells, J. Neuroimmunol. 124 (2002) 29–35.

[5] N.G. Carlson, W.A. Wieggel, J. Chen, A. Bacchi, S.W. Rogers, L.C. Gahring, Inflammatory cytokines IL-1 alpha, IL-1 beta, IL-6, and TNF-alpha impart neuroprotection to an excitotoxin through distinct pathways, J. Immunol. 163 (1999) 3963–3968.
[6] R. Diem, M. Hobom, P. Grotsch, B. Kramer, M. Bahr, Interleukin-1 beta protects neurons via the interleukin-1 (IL-1) receptor-mediated Akt pathway and by IL-1 receptor-independent decrease of transmembrane currents in vivo, Mol. Cell. Neurosci. 22 (2003) 487–500.
[7] J.L. Mason, K. Suzuki, D.D. Chaplin, G.K. Matsushima, Interleukin-1beta promotes repair of the CNS, J. Neurosci. 21 (2001) 7046–7052.
[8] D. Lindholm, R. Heumann, M. Meyer, H. Thoenen, Interleukin-1 regulates synthesis of nerve growth factor in non-neuronal cells of rat sciatic nerve, Nature 330 (1987) 658–659.
[9] H. Neumann, R. Schweigreiter, T. Yamashita, K. Rosenkranz, H. Wekerle, Y.A. Barde, Tumor necrosis factor inhibits neurite outgrowth and branching of hippocampal neurons by a rho-dependent mechanism, J. Neurosci. 22 (2002) 854–862.
[10] Z. Cao, Y. Gao, J.B. Bryson, J. Hou, N. Chaudhry, M. Siddiq, J. Martinez, T. Spencer, J. Carmel, R.B. Hart, M.T. Filbin, The cytokine interleukin-6 is sufficient but not necessary to mimic the peripheral conditioning lesion effect on axonal growth, J. Neurosci. 26 (2006) 5565–5573.
[11] H. Horie, I. Sakai, Y. Akahori, T. Kadoya, IL-1 beta enhances neurite regeneration from transected-nerve terminals of adult rat DRG, Neuroreport 8 (1997) 1955–1959.
[12] M. Lehmann, A. Fournier, I. Selles-Navarro, P. Dergham, A. Sebok, N. Leclerc, G. Tigyi, L. McKerracher, Inactivation of Rho signaling pathway promotes CNS axon regeneration, J. Neurosci. 19 (1999) 7537–7547.
[13] G. Yiu, Z. He, Glial inhibition of CNS axon regeneration, Nat. Rev. Neurosci. 7 (2006) 617–627.
[14] H. Higuchi, T. Yamashita, H. Yoshikawa, M. Tohyama, Functional inhibition of the p75 receptor using a small interfering RNA, Biochem. Biophys. Res. Commun. 301 (2003) 804–809.
[15] H. Tanaka, T. Yamashita, M. Asada, S. Mizutani, H. Yoshikawa, M. Tohyama, Cytoplasmic p21(Cip1/WAF1) regulates neurite remodeling by inhibiting Rho-kinase activity, J. Cell. Biol. 158 (2002) 321–329.
[16] T. Yamashita, M. Tohyama, The p75 receptor acts as a displacement factor that releases Rho from Rho-GDI, Nat. Neurosci. 6 (2003) 461–467.
[17] T. Omura, K. Omura, M. Sano, T. Sawada, T. Hasegawa, A. Nagano, Spatiotemporal quantification of recruit and resident macrophages after crush nerve injury utilizing immunohistochemistry, Brain Res. 1057 (2005) 29–36.
[18] N. Rothwell, Interleukin-1 and neuronal injury: mechanisms, modification, and therapeutic potential, Brain Behav. Immun. 17 (2003) 152–157.
[19] S. Tang, J. Qiu, E. Nikulina, M.T. Filbin, Soluble myelin-associated glycoprotein released from damaged white matter inhibits axonal regeneration, Mol. Cell. Neurosci. 18 (2001) 259–269.
[20] C.D. Nobes, A. Hall, Rho, rac, and cdc42 GTPases regulate the assembly of multimolecular focal complexes associated with actin stress fibers, lamellipodia, and filopodia, Cell 81 (1995) 53–62.
[21] E.E. Govek, S.E. Newey, L. Van Aelst, The role of the Rho GTPases in neuronal development, Genes Dev. 19 (2005) 1–49.
[22] M. Domeniconi, N. Zampieri, T. Spencer, M. Hilaire, W. Mellado, M.V. Chao, M.T. Filbin, MAG induces regulated intramembrane proteolysis of the p75 neurotrophin receptor to inhibit neurite outgrowth, Neuron 46 (2005) 849–855.
[23] B. Niederost, T. Oertle, J. Fritsche, R.A. McKinney, C.E. Bandtlow, Nogo-A and myelin-associated glycoprotein mediate neurite growth inhibition by antagonistic regulation of RhoA and Rac1, J. Neurosci. 22 (2002) 10368–10376.
[24] S.M. Allan, N.J. Rothwell, Cytokines and acute neurodegeneration, Nat. Rev. Neurosci. 2 (2001) 734–744.
[25] L. Liu, S.R. D'Mello, Phosphorylation of IkappaB-beta is necessary for neuronal survival, J. Biol. Chem. 281 (2006) 1506–1515.
[26] H. Gutierrez, V.A. Hale, X. Dolcet, A. Davies, NF-kappaB signalling regulates the growth of neural processes in the developing PNS and CNS, Development 132 (2005) 1713–1726.
[27] D. Srinivasan, J.H. Yen, D.J. Joseph, W. Friedman, Cell type-specific interleukin-1beta signaling in the CNS, J. Neurosci. 24 (2004) 6482–6488.
[28] G.X. Shi, J. Han, D.A. Andres, Rin GTPase couples nerve growth factor signaling to p38 and b-Raf/ERK pathways to promote neuronal differentiation, J. Biol. Chem. 280 (2005) 37599–37609.
[29] C. Huang, C.H. Borchers, M.D. Schaller, K. Jacobson, Phosphorylation of paxillin by p38MAPK is involved in the neurite extension of PC-12 cells, J. Cell. Biol. 164 (2004) 593–602.
[30] Z.Z. Gu, Y.C. Pan, J.K. Cui, M.J. Klebuc, S. Shenaq, P.K. Liu, Gene expression and apoptosis in the spinal cord neurons after sciatic nerve injury, Neurochem. Int. 30 (1997) 417–426.
[31] V. Guenard, C.A. Dinarello, P.J. Weston, P. Aebischer, Peripheral nerve regeneration is impeded by interleukin-1 receptor antagonist released from a polymeric guidance channel, J. Neurosci. Res. 29 (1991) 396–400.
[32] T. Wyss-Coray, L. Mucke, Inflammation in neurodegenerative disease—a double-edged sword, Neuron 35 (2002) 419–432.

Analysis of Radiocarpal and Midcarpal Motion in Stable and Unstable Rheumatoid Wrists Using 3-Dimensional Computed Tomography

Sayuri Arimitsu, MD, Kazuomi Sugamoto, MD, PhD, Jun Hashimoto, MD, PhD, Tsuyoshi Murase, MD, PhD, Hideki Yoshikawa, MD, PhD, Hisao Moritomo, MD, PhD

Purpose The kinematic evaluation of carpal motion, especially midcarpal motion, in rheumatoid arthritis (RA) has been extremely difficult because of limited imaging techniques previously available. The purpose of this study was to evaluate the amount of radiocarpal and midcarpal motion in the flexion-extension plane in both stable and unstable rheumatoid wrists using three-dimensional computed tomography.

Methods We acquired *in vivo* kinematic data on 30 wrists with RA by three-dimensional computed tomography with the wrist in 3 positions: neutral, maximum flexion, and maximum extension. All cases were radiographically classified into 1 of 2 subtypes, the stable form or unstable form, according to the classification by Flury et al. We evaluated the precise range of radiocarpal and midcarpal motion using a markerless bone registration technique and calculated the individual contributions to the total amount of wrist motion in the flexion-extension plane in the different radiographic subtypes of RA.

Results The average range of motion of radiocarpal and midcarpal joint was 27° ± 15 and 32° ± 17, respectively. The average contribution of midcarpal motion to the total amount of wrist motion was 54%. The average contribution of midcarpal motion in the unstable form was 67%, which was significantly higher than 47% ($p < .05$) in the stable form.

Conclusions Midcarpal motion of rheumatoid wrists in the flexion-extension plane was better preserved than previously thought. The contribution of midcarpal motion to the total amount of wrist motion was significantly greater ($p < .05$) in the unstable form than in the stable form of RA. *(J Hand Surg 2008;33A:189–197. Copyright © 2008 by the American Society for Surgery of the Hand.)*

Key words Kinematics, rheumatoid arthritis, three-dimensional, wrist.

Additional material is available online.

THE INVOLVEMENT OF THE WRIST in rheumatoid arthritis (RA) is common, and surgical treatment is often required to alleviate persistent wrist pain. The natural course of destruction in a rheumatoid wrist has been classified into 3 types by Simmen and Huber[1]: type I, the ankylosis type; type II, the osteoarthritis type; and type III, the disintegrating type. Based on their radiologic analysis, type I has a spontaneous tendency to progress into ankylosis, type II resembles secondary osteoarthritic changes as destruction progresses, and type III has progressive destruction, loss of alignment, and finally complete collapse of the wrist.[1] In addition, Flury et al[2] proposed the classification of wrists with RA into a stable form of the disease (types I and II) and an unstable form of disease (type III) to make the choice and timing of surgical intervention easier (Table 1 and Fig. 1). It has generally been thought that the deterioration of midcarpal joint is more severe in the unstable form than in the stable form.[3] Therefore, the partial arthrodesis technique, like radiolunate (RL) arthrodesis, has been applicable to the stable form, whereas the unstable form has been better treated by total arthrodesis of the wrist.[3]

Radiolunate arthrodesis is a well-established procedure for the RA wrists, and several researchers have reported the favorable clinical results of the procedure.[2–12] It has been suggested that RL arthrodesis is most useful in those

Department of Orthopaedic Surgery, Osaka University Graduate School of Medicine, Osaka, Japan.

The authors acknowledge the assistance during parts of the experimental procedure of Tetsuya Tomita, MD, PhD, Akira Goto, MD, PhD, Kunihiro Oka, MD, PhD, and Ryoji Nakao, Department of Orthopaedic Surgery, Osaka University Graduate School of Medicine.

Received for publication June 13, 2007; accepted in revised form November 15, 2007.

The authors received support from the Japan Science and Technology Agency.

Corresponding author: Sayuri Arimitsu, MD, Department of Orthopaedic Surgery, Osaka University Graduate School of Medicine, 2-2, Yamada-oka, Suita, Osaka 565-0871, Japan; e-mail: sayu@df6.so-net.ne.jp.

0363-5023/08/33A02-0007$34.00/0
doi:10.1016/j.jhsa.2007.11.012

TABLE 1: Classification by the Natural Course of the Rheumatoid Wrist and the Radiologic Parameters Described by Simmen and Huber[1] and Flury et al[2]

	Classification		Radiologic Parameters	
	Simmen and Huber[1]	Flury et al[2]	Ulnar Carpal Translocation* (mm)	Loss of Carpal Height Ratio*
Type I	Ankylosis	Stable form	3.7 (0–11)	Δ0.14 (0.01–0.28)
Type II	Osteoarthritis	Stable form	3.8 (0–8)	Δ0.16 (0.02–0.34)
Type III	Disintegration	Unstable form	9.5 (4–17)	Δ0.30 (0.10–0.46)

*The radiologic parameters 10 to 20 years after onset of RA represented by Simmen and Huber[1] (n = 126).

rheumatoid patients whose disease had left the midcarpal joints relatively unaffected as seen on the radiograph.[1] However, the preoperative evaluation of the midcarpal joint on the radiograph has been difficult because of the complicated and overlapping shapes of the carpal bones in RA deformities. Recently, researchers have been able to measure *in vivo* and three-dimensional (3-D) kinematics of the human joint using a markerless bone registration technique, which is a method for evaluating the precise motions by determining relative positions of bones in different volume images.[13–19] We thought it would be possible to evaluate the kinematics of the carpal motion and quantify the midcarpal motion preoperatively in cases of RA with this 3-D technique.

The kinematic behavior of the carpal bones in rheumatoid wrist is not well-known, especially in relation to the RA subtypes. The purpose of this study was to evaluate the amount of radiocarpal and midcarpal motion in the flexion-extension plane in both stable and unstable rheumatoid wrists using 3-D computed tomography (3-D CT). We calculated the individual contributions of radiocarpal and midcarpal motion to the total amount of wrist motion to determine which radiographic subtype of RA had the greater contribution of midcarpal motion to the total amount of wrist motion.

MATERIALS AND METHODS

Subjects

We randomly selected 30 wrists from 29 RA patients who were regularly treated with medication at our institution. All of them had pain and instability of the wrists. One patient was a man and 28 were women. The average age was 60 years (range, 21 to 80 years). The average duration of RA was 13 years (range, 6 to 38 years). For comparison, we investigated a control group of 10 normal wrists from 10 healthy volunteers comprising 8 men and 2 women whose average age was 29 years (range, 22 to 36 years). All subjects consented to be included in this study.

Radiographic Evaluation

To investigate the relationship between the contribution of midcarpal motion to the total amount of wrist motion and the radiographic appearance of RA, we classified 30 wrists with RA into 1 of the 2 subtypes, the stable form or the unstable form of the disease, by the natural course of the rheumatoid wrist and the radiologic parameters (Table 1 and

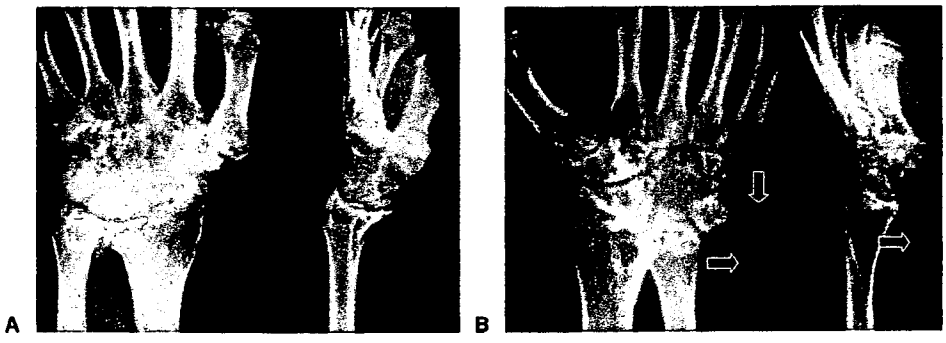

FIGURE 1: The [A] stable form and [B] unstable form of RA by the method of Flury et al.[2] [A] Representative case of the stable form of RA, which has a spontaneous tendency to progress into ankylosis (Video 1, a 3-dimensional animation of a representative case of the stable form of RA wrist, may be viewed at the *Journal's* Web site, www.jhandsurg.org). [B] Representative case of the unstable form of RA in which there is progressive destruction and loss of alignment. The carpal height is reduced and the carpal bones are dislocated ulno-palmarly with respect to the case shown in [A] (arrows) (Video 2, a 3-dimensional animation of a representative case of the unstable form of RA wrist, may be viewed at the *Journal's* Web site, www.jhandsurg.org).

Fig. 1).[1,2] The radiographic parameters we used for classification were ulnar translocation and carpal height ratio (Table 1).[1] In the current study, we also investigated our cases with or without scaphoid-lunate (S-L) dissociation (the gap between scaphoid and lunate is more than 2 mm[12] on the anteroposterior radiograph) in relation to the radiographic subtypes of RA.

Image Acquisition

The technique we used for *in vivo* 3-D kinematic evaluation has been described in detail previously.[14–19] For patients with RA, we performed 3-D CT on the wrists using a clinical helical type scanner with an image slice thickness of 0.625 mm (LightSpeed Ultra16; General Electric, Waukesha, WI). For the normal wrists of volunteers, magnetic resonance images were obtained using a 1.5-T commercial magnetic resonance imaging (MRI) system (Magnetom Vision PlusR 1.5T MRI; Siemens, Munich, Germany) in conjunction with a receive-only surface coil of 2.3 ms/33 ms, a flip angle of 45°, a 160-mm field of view, and 0.5-mm-thick contiguous slices, with 0.6 × 0.8 mm pixels. For each wrist, we acquired image with the wrist in 3 different positions: neutral (in which the third metacarpal and the forearm axis were aligned), maximum wrist flexion, and maximum wrist extension. For normal volunteers, we used a custom-made device to hold the position during image acquisition. However, we could not use the device for RA patients because of pain and deformity of the wrists. Data were saved in a standard format (Digital Imaging and Communications in Medicine [DICOM]) that is used commonly for transferring and storing medical images.

Segmentation and Construction of a 3-D Surface Bone Model

Segmentation was defined as extracting bone regions individually. The anatomic structure or region of interest must be delineated and separated so that it can be viewed individually and 3-D bone models can be reconstructed. Regions of individual bones were segmented semiautomatically using a software program for image analysis (Virtual Place-M; AZE, Ltd., Tokyo, Japan). The software generated 3-D surface bone models using the marching cubes technique.[14,15,20]

Registration

We created 3-D bone models and quantitatively evaluated the motion of the midcarpal joint using a markerless volume-based registration technique. The kinematic variables were calculated by registering the bone, obtained by segmentation, from one position to another. The accuracy of volume-based registration has been discussed previously,[14,15] the mean rotation error was 1° ± 1, and the mean translation error was 0.21 mm ± 0.25.

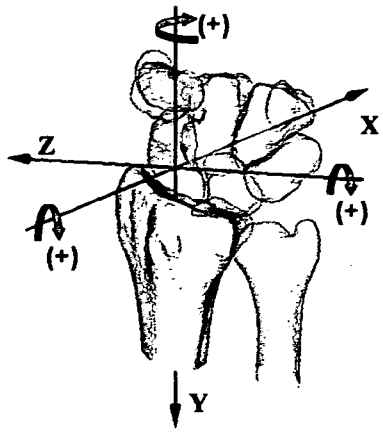

FIGURE 2: A consistent orthogonal reference system established in the radius.

Three-Dimensional Quantification of the Range of Motion

To quantify the 3-D range of motion of the midcarpal joint, we defined the grid for the radius, which was the orthogonal reference system advocated by Belsole et al (Fig. 2).[15,21,22] The total amount of wrist motion in the flexion-extension plane was defined as the total range of motion of the radiocarpal and midcarpal joint in the flexion-extension plane, which was evaluated by assessing the range of capitate motion relative to the reference system established on the radius. The range of radiocarpal motion in the flexion-extension plane was investigated by that of the lunate motion. Then the range of the midcarpal motion in the flexion-extension plane could be quantified as the difference between the total amount of wrist motion and the range of radiocarpal motion.

In the flexion-extension motion of the wrist, the radiocarpal and midcarpal joints have motions in planes other than the flexion-extension plane such as the pronation/supination (P/S) plane and the radial/ulnar deviation (RD/UD) plane. There are coupling motions associated with wrist motion in the flexion-extension plane. We defined the 2 motions in the other planes as *out of the plane motion (P/S)* and *out of the plane motion (RD/UD)*, respectively. We quantified the amount of wrist motion in the flexion-extension plane and out of the plane separately for the radiocarpal and midcarpal joints.

A consistent orthogonal reference system was established in the radius as follows.[22] The y axis was defined as the longitudinal radial axis and indicated the proximal (+)/distal (–) direction. The z axis was defined as the line running through the styloid process on the plane perpendicular to the y axis and indicated the radial (+)/ulnar (–) direction. The x axis was defined as the line perpendicular to the yz plane and indicated the palmar (+)/dorsal (–) direction. Rotation around the z axis produced flexion (+)/extension (–), rotation around the y axis was pronation (+)/supination (–), and rotation around the x axis was ulnar (+)/radial (–)

deviation (Fig. 2). We defined the rotating angle of the carpus around each of the 3 axes as the range of wrist motion.

Evaluation of the Contribution Ratio

We also evaluated the individual contributions of radiocarpal and midcarpal motion to the total amount of wrist motion. We defined *contribution ratio* as the percentage of the range of radiocarpal motion or midcarpal motion relative to the total amount of wrist motion. In this study, the contribution ratio was investigated only in the flexion-extension plane.

Statistical Analysis

All data were expressed as the mean with the standard deviation. Quantitative comparison of results between the control group and the RA group was performed using standard statistical formulas based on the Mann-Whitney U test. Results were deemed to be significant if $p < .05$.

RESULTS

Rheumatoid Arthritis Versus Normal

In the rheumatoid wrists, the average of total amount of wrist motion in the flexion-extension plane was 59° ± 20. The average range of radiocarpal motion in the flexion-extension plane was 27° ± 15 and that of midcarpal motion was 32° ± 17. In the normal wrists, the average of total amount of wrist motion in the flexion-extension plane was 111° ± 15. The average range of radiocarpal motion in the flexion-extension plane was 63° ± 14° and that of midcarpal motion was 47° ± 8. The ranges of radiocarpal motion ($p < .01$) and midcarpal motion ($p < .01$) in the flexion-extension plane in RA wrists were significantly less than normal as expected (Table 2). The average contribution ratios of radiocarpal and midcarpal joint in the flexion-extension plane were 46% and 54%, respectively, in RA wrists and 57% and 43%, respectively, in normal wrists (Fig. 3). On average, the midcarpal joint tended to have a greater contribution in the flexion-extension plane in RA wrists compared with normal wrists, even though the difference was not significant ($p = .179$).

Regarding the out of the plane motion of the wrists, the average of total amount of out of the plane motion (P/S) in RA was 8° ± 11 in supination during flexion motion of the wrist. The average range of out of the plane motion (P/S) in the radiocarpal joint was 5° ± 7 and that in the midcarpal joint was 2° ± 8 in supination during flexion motion of the wrists. In the normal wrists, the average of total amount of out of the plane motion (P/S) was 8° ± 13 in pronation during flexion motion of the wrists. The average range of out of the plane motion (P/S) in the radiocarpal joint was 3° ± 6 and that in the midcarpal joint was 4° ± 9 in pronation during flexion motion of the wrists. Consequently, during flexion motion of the wrists, the radiocarpal joint ($p < .01$) and the whole wrist joint, that is, the total for the radiocarpal and midcarpal joints ($p < .01$), significantly supinated in RA wrists compared with normal (Table 2).

The average of total amount of out of the plane motion (RD/UD) in RA was 5° ± 8 in ulnar deviation during flexion motion of the wrists. The average of out of the plane motion (RD/UD) in the radiocarpal joint was 1° ± 7 and that in the midcarpal joint was 4° ± 8 in ulnar deviation during flexion motion of the wrists. In the normal wrists, the average of total amount of out of the plane motion (RD/UD) was 8° ± 13 in radial deviation during flexion motion of the wrists. The average range of out of the plane motion (RD/UD) in the radiocarpal joint was 4° ± 8 and that in the midcarpal joint was 4° ± 8 in radial deviation during flexion motion of the wrists. Consequently, during flexion motion of the wrists, the midcarpal joint ($p < .05$) and the whole wrist joint, that is, the total for the radiocarpal and midcarpal joints ($p < .01$), significantly deviated ulnarly in RA wrists compared with normal (Table 2).

Stable Form Versus Unstable Form of RA

We classified the 30 rheumatoid wrists into 19 cases of stable form of disease and 11 cases of unstable form. The average of total ulnar translocation after onset of RA was 4.1 mm in the stable form and 10.7 mm in the unstable form; these values are consistent with the radiographic parameters described by Simmen and Huber (Table 1).[1] The average of total loss of carpal height ratio after onset of RA was 0.12 in the stable form and 0.28 in the unstable form; these values are also consistent with the radiographic parameters described by Simmen and Huber (Table 1).[1] Among the 11 wrists in the unstable form of disease, 7 showed S-L dissociation. In contrast, S-L dissociation was not found among the 19 wrists in the stable form of disease.

The range of radiocarpal and midcarpal motions in the flexion-extension plane varied greatly among cases in the stable form of disease (Fig. 4). In contrast, the range in cases of the unstable form was relatively constant; in 8 of the 11 wrists in unstable form, the midcarpal motion in the flexion-extension plane was greater than radiocarpal motion (Figs. 4, 5). Only 3 cases of the unstable form had greater motion in the radiocarpal joint than in the midcarpal joint (Fig. 4). The average ranges of radiocarpal and midcarpal motion in the flexion-extension plane were 31° ± 16 and 28° ± 15, respectively, in the stable form, and 20° ± 12 and 38° ± 19, respectively, in the unstable form. In the radiocarpal joint, the range of motion of the unstable form in the flexion-extension plane was significantly less than that of the stable form ($p < .05$), whereas in the midcarpal joint, there was no significant difference ($p < .05$) between the 2 groups (Table 3). The average contribution ratios of radiocarpal and midcarpal joint in the flexion-extension plane were 53% and 47%, respectively, in the stable form and 33% and 67%, respectively, in the unstable form (Fig. 6). In the midcarpal joint, the contribution ratio of the unstable-form group in the flexion-extension plane was significantly greater than that of the stable-form group ($p < .05$).

Regarding out of the plane motion (P/S) of the rheumatoid wrists, during flexion motion of the wrists, the

TABLE 2: Kinematic Data During Flexion Motion of the Wrists: RA Versus Normal Wrists

	Range of Motion During the Flexion Motion of the Wrists (°)								
	In the Flexion-Extension Plane Motion			Out of the Flexion-Extension Plane Motion					
	Flexion (+)/Extension (–)			Pronation (+)/Supination (–)			Ulnar (+)/Radial (–) Deviation		
	Radiocarpal Motion	Midcarpal Motion	Total Amount of Motion	Radiocarpal Motion	Midcarpal Motion	Total Amount of Motion	Radiocarpal Motion	Midcarpal Motion	Total Amount of Motion
Normal (n = 10)									
Average	63	47	111	3	4	8	–4	–4	–8
SD	14	8	15	6	9	13	8	8	13
RA (n = 30)									
Average	27**	32**	59**	–5**	–2	–8**	1	4*	5**
SD	15	17	20	7	8	11	7	8	8

*$p < .05$, **$p < .01$ versus normal.

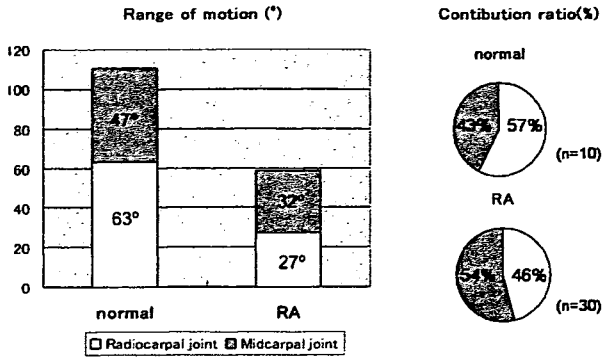

FIGURE 3: Average range of motion and contribution ratios of the radiocarpal and midcarpal joint in the flexion-extension plane in normal and RA wrists. The contribution ratio is the percentage contribution of radiocarpal or midcarpal motion relative to the total amount of wrist motion.

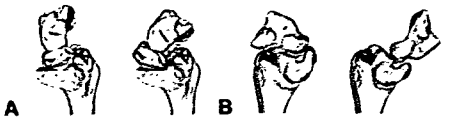

FIGURE 5: Flexion-extension motions of the lunate and capitate relative to the radius in the stable and unstable forms of RA wrists, viewed from the ulnar side. A Representative case of the stable form of RA, shown in Figure 1A, in which the range of motion in the flexion-extension plane was 40° in the radiocarpal joint and 5° in the midcarpal joint (Video 1, a 3-dimensional animation of a representative case of the stable form of RA wrist, may be viewed at the *Journal's* Web site, www.jhandsurg.org). B Representative case of the unstable form of RA, shown in Figure 1B, in which the range of motion in the flexion-extension plane was 37° in the radiocarpal joint and 83° in the midcarpal joint (Video 2, a 3-dimensional animation of a representative case of the unstable form of RA wrist, may be viewed at the *Journal's* Web site, www.jhandsurg.org).

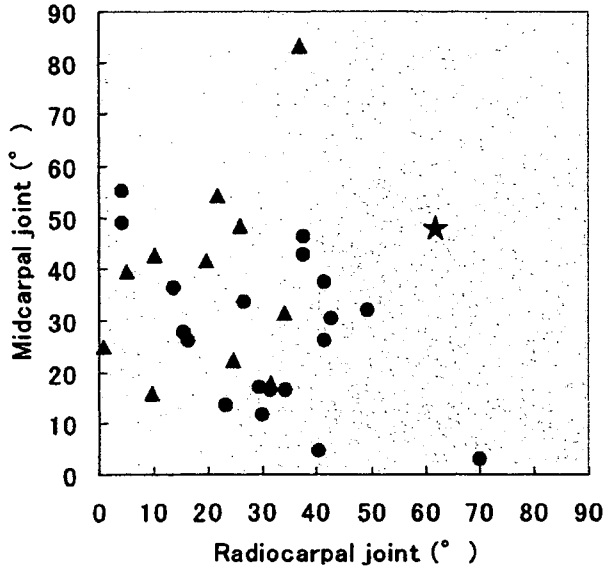

FIGURE 4: Scattering diagram of the range of the radiocarpal and midcarpal motion in the flexion-extension plane in stable and unstable forms of RA wrists and in normal wrists: ●, stable form of RA (19 cases); ▲, unstable form of RA (11 cases); ★, average range of motion in 10 normal wrists (63° in the radiocarpal joint and 47° in the midcarpal joint).

midcarpal joint ($p < .05$) and the whole wrist joint, that is, the total for the radiocarpal and midcarpal joints ($p < .01$), significantly supinated in the unstable-form group compared with the stable-form group. Regarding out of the plane motion (RD/UD), we found no significant difference ($p < .05$) between the 2 groups (Table 3).

DISCUSSION

Kinematic evaluation of rheumatoid wrists by x-ray has been difficult because of the complicated and overlapping shapes of the carpal bones. In the current study, we quantitatively evaluated the amount of radiocarpal and midcarpal motion in the flexion-extension plane of the rheumatoid wrists using 3-D CT. We also elucidated the relationship between the contribution of midcarpal motion to the total amount of wrist motion in the flexion-extension plane and the radiographic subtypes of RA.

We found that the contribution of midcarpal motion to the total amount of wrist motion in the flexion-extension plane was significantly greater in the unstable form than in the stable form of RA (Table 3 and Fig. 6). This result may seem counterintuitive because of the radiographic appearance of the unstable form of RA in which all parts of the wrist joints are severely damaged. We speculate that our results can be accounted for mainly by stronger skeletal constraints in the midcarpal joint than in the radiocarpal joint. The midcarpal joint has its own self-stabilizing mechanism; when the trapezium is axially loaded against the scaphoid, the flexion moment by the scaphoid is constrained by the extension moment experienced by the triquetrum, and stable equilibrium is achieved.[19] Moreover, the midcarpal joint is proved to have an adaptive mechanism whereby the concave and convex joint surfaces allow preservation of articular congruity.[19] On the other hand, the stability of the radiocarpal joint depends on ligamentous constraints. In the radiocarpal joint, the carpal bones tend to slide ulno-palmarward on the sloping plane of the distal radius, and the displacement is resisted by the palmar and dorsal radiotriquetral and palmar RL ligaments.[22] It is likely that the radiocarpal joint in which joint stability depends on ligamentous constraints easily loses its stability, particularly in the unstable form of RA.

Scapholunate dissociation can be associated with RA wrist by the multiple laxities of ligaments including the dorsal scapholunate ligament, especially in the unstable form of RA. In the current study, S-L dissociation occurred in 7 of 11 wrists in the unstable form of RA; however, it did not occur in any of the 19 wrists in the stable form. This may have the relationship to our results that the range of

TABLE 3: Kinematic Data During Flexion Motion of the Wrists: Stable Versus Unstable Forms of RA

	Range of Motion During the Flexion Motion of the Rheumatoid Wrists (°)								
	In the Flexion-Extension Plane Motion			Out of the Flexion-Extension Plane Motion					
	Flexion (+)/Extension (–)			Pronation (+)/Supination (–)			Ulnar (+)/Radial (–) Deviation		
	Radiocarpal Motion	Midcarpal Motion	Total Amount of Motion	Radiocarpal Motion	Midcarpal Motion	Total Amount of Motion	Radiocarpal Motion	Midcarpal Motion	Total Amount of Motion
Stable form (n = 19)									
Average	31	28	59	–3	0	–3	2	3	5
SD	16	15	15	5	7	9	5	7	7
Unstable form (n = 11)									
Average	20*	38	58	–9	–7*	–16**	1	6	7
SD	12	19	25	9	7	10	8	9	9

*$p < .05$, **$p < .01$ versus stable form.

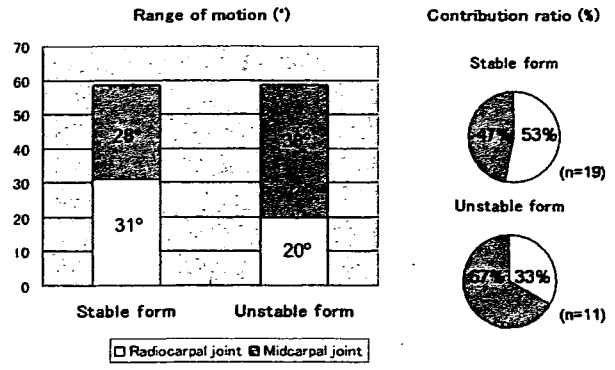

FIGURE 6: Average range of motion and the contribution ratios of the radiocarpal and midcarpal joints in the flexion-extension plane in the stable and unstable forms of RA wrists. The contribution ratio is the percentage of the contribution of the radiocarpal motion or midcarpal motion relative to the total amount of wrist motion.

radiocarpal motion in the unstable form in the flexion-extension plane was significantly less than that in the stable form. In the normal wrists, if the interosseous ligament between scaphoid and lunate is disrupted, the scaphoid tends to flex and the lunate tends to extend and the congruity of the radiocarpal joint is lost.[23] These tendencies may lead to the loss of the range of radiocarpal motion.

Regarding the motion of the wrists outside the flexion-extension plane, we found RA wrists significantly deviated ulnarly during flexion motion compared with normal (Table 2). This may be related to the unique motion patterns of the midcarpal joint. It has been reported that the essential plane of motion of the midcarpal joint is oblique to the anatomic planes, which corresponds with extension with radial deviation and flexion with ulnar deviation—the so-called dart-throwing motion.[19] Under the severe destruction of the radiocarpal joint in RA, especially in the unstable form, it is possible that the preserved midcarpal function facilitates the dart-throwing motion rather than the pure flexion-extension motion. This dart-throwing motion seems to be helpful for patients with RA because the oblique motion is used in performing many tasks of daily living such as hair combing, washcloth wringing, shoe tying, and can-opening.[24,25]

Most clinical reports have asserted that osseous procedures such as partial fusions of compartments of the joint are recommended to stabilize wrists with RA.[1] It has been suggested that RL arthrodesis is indicated only in the middle stage of the osteoarthritis type of RA and that other types such as the unstable form of RA may be better treated by total wrist arthrodesis.[3] However, reconsideration is needed because total wrist arthrodesis involves considerable loss of wrist function. Borisch and Haussmann[10] reported that the RL arthrodesis was able to reestablish the midcarpal joint and that the carpus showed an amazing capacity of adaptation. Ishikawa et al[11] suggested that radiocarpal fusion resulted in good stability with preservation of motion despite radiographic progression of the disease. Our results showing that the midcarpal motion in the unstable form of RA was better preserved than previously thought may support more positive application of RL arthrodesis in certain cases with the unstable form of RA. However, our results do not predict wrist function perfectly after RL arthrodesis in ongoing disease, because previous researchers reported that although the midcarpal joint space was generally preserved after radiocarpal arthrodesis, some wrists lost the joint space and became stiff.[9,11]

The current study has some limitations. The most important limitation is that we compared data on patients with RA based on CT images with data on normal volunteers based on MRI. However, we quantified the range of joint motion as the rotational angle of the carpus relative to a reference system established in the radius. The way in which the images are acquired may not affect the overall results if it is under the accuracy of volume-based registration. A second limitation of this study is that the patients with RA wrists were not fully matched for age and gender with the normal-wrist volunteers. The results might have been different if these demographic parameters of the study groups were identical. A further limitation is that during image acquisition, we were unable to use the position-holding device in the RA patients to maintain the neutral, maximum flexion, and extension positions because of symptomatic pain and wrist deformity. Because the patients used their own muscle power to hold their wrists in position, the positions recorded may not have been precisely maximum flexion and maximum extension.

Nevertheless, the results of this study may be useful in establishing a treatment plan in advanced cases of RA. Even some cases in the stable form of RA wrist may be treated by RL fusion, particularly the cases in which the midcarpal joint space is not visible on x-ray but the midcarpal motion is preserved under the 3-D investigation. Based on our findings of the preservation of a great amount of motion at the midcarpal joint in rheumatoid patients with symptomatic wrists, we believe that our study rationally supports the application of RL arthrodesis rather than total wrist arthrodesis as treatment in appropriate RA patients.

REFERENCES

1. Simmen BR, Huber H. The rheumatoid wrist: a new classification related to the type of the natural course and its consequences for surgical therapy. In: Simmen BR, Hagena FW, eds. The wrist in rheumatoid arthritis. Rheumatology. Basel: Karger, 1992:13–25.
2. Flury MP, Herren DB, Simmen BR. Rheumatoid arthritis of the wrist. Classification related to the natural course. Clin Orthop 1999;366:72–77.
3. Della Santa D, Chamay A. Radiological evolution of the rheumatoid wrist after radio-lunate arthrodesis. J Hand Surg 1995;20B:146–154.
4. Chamay A, Della Santa D, Vilaseca A. Radiolunate arthrodesis. Factor of stability for the rheumatoid wrist. Ann Chir Main 1983;2:5–17.
5. Linscheid RL, Dobyns JH. Radiolunate arthrodesis. J Hand Surg 1985;10A:821–829.

6.Stanley JK, Boot DA. Radiolunate arthrodesis. J Hand Surg 1989;14B:283–287.
7.Ishikawa H, Hanyu T, Saito H, Takahashi H. Limited arthrodesis for the rheumatoid wrist. J Hand Surg 1992;17A: 1103–1109.
8.Halikis MN, Colello-Abraham K, Taleisnik J. Radiolunate fusion. The forgotten partial arthrodesis. Clin Orthop 1997; 341:30–35.
9.Doets HC, Raven EEJ. Radiolunate arthrodesis. A procedure for stabilizing and preserving mobility in the arthritic wrist. J Bone Joint Surg 1999;81B:1013–1016.
10.Borisch N, Haussmann P. Radiolunate arthrodesis in the rheumatoid wrist: a retrospective clinical and radiological long-term follow-up. J Hand Surg 2002;27B:61–72.
11.Ishikawa H, Murasawa A, Nakazono K. Long-term follow-up study of radiocarpal arthrodesis for the rheumatoid wrist. J Hand Surg 2005;30A:658–666.
12.Muramatsu K, Ihara K, Tanaka H, Kawai S. Carpal instability in rheumatoid wrists. Rheumatol Int 2004;24:34–36.
13.Besl PJ, Mackay N. A method for registration of 3-D shapes. IEEE Trans Pattern Anal 1992;14:239–256.
14.Goto A, Moritomo H, Murase T, Oka K, Sugamoto K, Arimura T, et al. In vivo three-dimensional wrist motion analysis using magnetic resonance imaging and volume-based registration. J Orthop Res 2005;23:750–756.
15.Oka K, Moritomo H, Murase T, Goto A, Sugamoto K, Yoshikawa H. Patterns of carpal deformity in scaphoid nonunion: a three-dimensional and quantitative analysis. J Hand Surg 2005;30A:1136–1144.
16.Oka K, Doi K, Suzuki K, Murase T, Goto A, Yoshikawa H, et al. In vivo three-dimensional motion analysis of the forearm with radioulnar synostosis treated by the Kanaya procedure. J Orthop Res 2006;24:1028–1035.
17.Moritomo H, Goto A, Sato Y, Sugamoto K, Murase T, Yoshikawa H. The triquetrum-hamate joint: an anatomic and in vivo three-dimensional kinematic study. J Hand Surg 2003;28A:797–805.
18.Moritomo H, Murase T, Goto A, Oka K, Sugamoto K, Yoshikawa H. Capitate-based kinematics of the midcarpal joint during wrist radioulnar deviation: an in vivo three-dimensional motion analysis. J Hand Surg 2004;29A:668–675.
19.Moritomo H, Murase T, Goto A, Oka K, Sugamoto K, Yoshikawa H. In vivo three-dimensional kinematics of the midcarpal joint of the wrist. J Bone Joint Surg 2006;88A: 611–621.
20.Lorensen WE, Cline HE. Marching cubes: a high resolution 3D surface construction algorithm. Computer Graphics 1987;21:163–169.
21.Belsole RJ, Hilbelink DR, Llewellyn JA, Dale M, Ogden JA. Carpal orientation from computed reference axes. J Hand Surg 1991;16A:82–90.
22.Arimitsu S, Murase T, Hashimoto J, Oka K, Sugamoto K, Yoshikawa H, et al. A three-dimensional quantitative analysis of carpal deformity in rheumatoid wrists. J Bone Joint Surg 2007;89B:490–494.
23.Linscheid RL, Dobyns JH, Beckenbaugh RD, Cooney WP, Wood MB. Instability patterns of the wrist. J Hand Surg 1983;8:682–686.
24.Li ZM, Kuxhaus L, Fisk JA, Christophel TH. Coupling between wrist flexion-extension and radial-ulnar deviation. Clin Biomech (Bristol, Avon) 2005;20:177–183.
25.Palmer AK, Werner FW, Murphy D, Glisson R. Functional wrist motion: a biomechanical study. J Hand Surg 1985;10A: 39–46.

Numerical analysis of cooperative abduction muscle forces in a human shoulder joint

Naomi Oizumi, MD,[a] Shigeru Tadano, PhD,[b] Youichi Narita, ME,[b] Naoki Suenaga, MD,[a] Norimasa Iwasaki, MD,[a] and Akio Minami, MD,[a] *Sapporo, Japan*

Because some shoulder muscles originate from a wide area, the modeling of such muscles has been a significant problem in a computer simulation. We demonstrated a new method of determining a vector for each of the muscles originating from a wide area. A 3-dimensional musculoskeletal model of a human shoulder was constructed from computed tomography data of a normal volunteer. Numerical analysis of 11 muscle forces and the joint reaction force during shoulder abduction from 10° to 150° was performed from the static equilibrium equations. An optimal origin point for the vector of the muscle with a wide origin area was determined in every analyzed position. Electromyography was carried out to validate the results of the simulation, and a significant correlation with the analyzed force was obtained in each muscle. The anatomic biomechanical model with the new muscle modeling method led to the results reflecting the actual muscle activities in a living body. (J Shoulder Elbow Surg 2006;15:331-338.)

To evaluate activities of muscles surrounding a shoulder joint, electromyography (EMG) has been widely used for a long period.[2,8,14,15] However, EMG has several disadvantages: it is invasive, it is difficult to insert a needle into the proper position in some muscles, and most importantly, it is unable to quantify individual muscle forces. Cadaveric models have also been used to simulate joint motions in various conditions.[12] However, it is difficult to reproduce 3-dimensional motions of the scapula and humerus because they have to be fixed on a device. Therefore, the experimental analyses are often limited to the glenohumeral joint, and muscles originating from the thorax are excluded from the examination. For these reasons, computer simulation has come to be a valuable method in the analysis of shoulder muscle forces.[5,7,11,17]

The combined motion of 3 joints (glenohumeral, acromioclavicular, and sternoclavicular joints) allows the shoulder joint to have the widest range of motion among all joints in the human body. Bony stability of the glenohumeral joint is minimal so that soft tissues, including ligaments, capsule, and muscles, that surround the joint play an important role in stabilization. Unlike other joints that have more bony stability, such as the hip joint, shoulder joint muscles act during any shoulder motion not only as a source of force but also as a stabilizer. In fact, more than 20 muscles (and their separate parts) act cooperatively during shoulder motion. Because of these anatomic features, it is important to build an anatomically accurate geometric model for a precise computer simulation of shoulder muscles. Some of the shoulder muscles, such as the deltoid, supraspinatus, infraspinatus, subscapularis, and so on, originate from a wide area, and modeling should be taken into consideration especially for these muscles. Modeling of muscles with a wide area of origin has been a significant subject of discussion, and various procedures were proposed in previous muscle force analyses.[4,16] In this study, we introduce a new modeling method for muscles with a wide origin area using computed tomography (CT) data of a shoulder joint in a normal volunteer. We created a 3-dimensional biomechanical model for analyzing muscle forces and validated the analyzed forces by comparing them with the EMG values.

MATERIALS AND METHODS

Biomechanical model

CT data of a shoulder in a normal volunteer (23-year-old man; body weight, 65 kg; length between shoulder and wrist joint, 55 cm) were prepared to create a 3-dimensional musculoskeletal model. The volunteer had neither a history of trauma nor any symptoms in his shoulder. Informed consent for participating in this study was obtained from the volunteer. Axial CT images of the shoulder, elbow, and forearm were scanned by a high-resolution helical scanner (CT Highspeed Advantage; GE Medical System, Milwau-

From the [a]Department of Orthopaedic Surgery, Hokkaido University School of Medicine, and [b]Division of Mechanical Science, Graduate School of Engineering, Hokkaido University.

Reprint requests: Naomi Oizumi, MD, Department of Orthopaedic Surgery, Hokkaido University School of Medicine, North 15, West 7 Kita-ku, Sapporo 060-8638, Japan (E-mail: nao9877@aol.com).

1058-2746/2006/$32.00
doi:10.1016/j.jse.2005.08.012

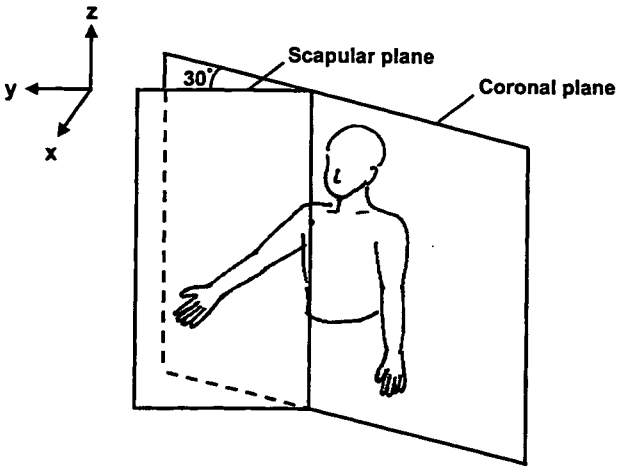

Figure 1 Three-dimensional coordinate system of model. Origin, Center of humeral head; x-axis, perpendicular to scapular plane; y-axis, horizontal on scapular plane; z-axis, vertical.

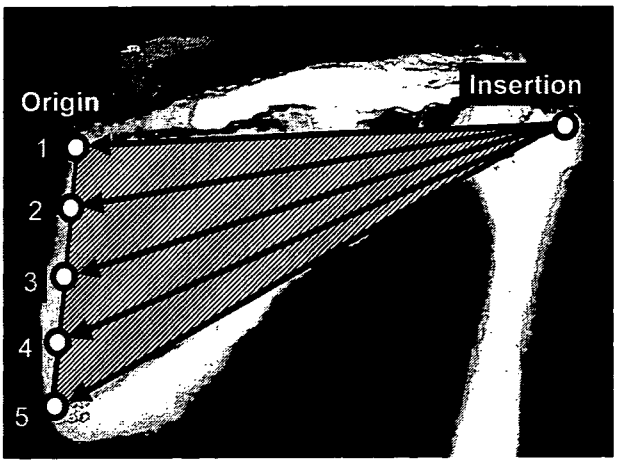

Figure 2 In the infraspinatus muscle, 5 possible origin points were set on the edge of the origin area at even intervals, and the adequate point was selected in each abduction angle by use of the optimization method.

kee, WI). The slice thickness and interval were set at 1 mm and the table speed at 1 mm/s. The upper extremity was placed at the side of the trunk, the shoulder joint was positioned in neutral rotation, and the elbow joint was positioned in full extension during imaging. The obtained images were transferred to a computer, and a 3-dimensional image was created by use of the medical image–analyzing software Analyze 3.0 (Biomechanical Imaging Resource, Rochester, MN). A 3-dimensional coordinate system was determined, with the center of the humeral head being considered as the origin (Figure 1). Each axis was determined as follows: x-axis, perpendicular to the scapular plane (a vertical plane 0° from a frontal plane); y-axis, horizontal on the scapular plane; and z-axis, vertical. Three-dimensional coordinates of the origin and insertion of each muscle were manually determined from muscle contours or anatomic bony landmarks (or both) on the 3 directional (coronal, sagittal, and axial) cross-sectional images. Every coordinate point was automatically placed on the surface of the bone. Eleven muscles that originate from the scapula and insert on the upper extremity (humerus, radius, and ulna) were included in this study. Those muscles were as follows: anterior fiber of deltoid (F1), middle fiber of deltoid (F2), posterior fiber of deltoid (F3), supraspinatus (F4), infraspinatus (F5), subscapularis (F6), teres minor (F7), teres major (F8), long head of biceps (F9), short head of biceps (F10), and long head of triceps (F11). The muscles were basically defined as a straight-line vector from the insertion to the origin. However, in muscles that originate from a wide area, it is quite unlikely that all muscle fibers transmit the force to the insertion equally during various movements. The most active muscle fibers should change as the joint position changes. Therefore, if these muscles are represented as a fixed straight-line vector, considerable errors may result in the analysis. For these reasons, we assumed that the primary active muscle fibers were approximated to a straight-line vector, which changed its direction in each abduction angle. On the basis of this assumption, we developed the following procedure. An origin line was determined on the edge of the origin area that was farthest from the insertion, and several possible origin points were set on the line at even intervals (Figure 2). Three points were set as possible origin points for each fiber of the deltoid and supraspinatus, and five points were set for the infraspinatus and subscapularis according to the approximate length of the origin line of each muscle. The optimal point in each abduction angle, which determined the direction of the muscle vector, was selected among these points by use of the optimization technique mentioned later. The insertion remained fixed in every muscle. By this procedure, an optimal muscle vector was determined in every abduction angle.

The proximal part of the long head of the biceps shows a unique morphology that originates from the glenoid rim as a tendon and runs along the surface of the humeral head. We set the contact point at the upper end of the bicipital groove and defined the muscle vector as a straight-line vector from the insertion to the contact point, as opposed to defining the vector from the insertion to the origin.

The middle fiber of the deltoid muscle is in a curved shape, wraps around the humeral head in small abduction angles (Figure 3, *A*), and becomes a linear shape as the arm abducts (Figure 3, *B*). Because the straight-line vector from its insertion to the origin penetrates the humerus in small abduction angles, we set the contact point on the greater tuberosity and defined the muscle vector as a vector from the insertion to the contact point as aforementioned. To determine the range of the abduction angle where the straight-line vector penetrates the bone, we carried out the following study: Magnetic resonance imaging data of the shoulders in 10 normal volunteers (8 men and 2 women), including the same volunteer whose CT data were used for the musculoskeletal model, were prepared. The mean age was 24.8 years (range, 24-39 years). All subjects had neither a history of trauma nor any symptoms in the examined shoulders. Informed consent for participating in this study was obtained. Oblique coronal (scapular-plane) views of the shoulders were scanned via an open magnetic resonance scanner (0.2-T Magnetom Open; Siemens, Er-

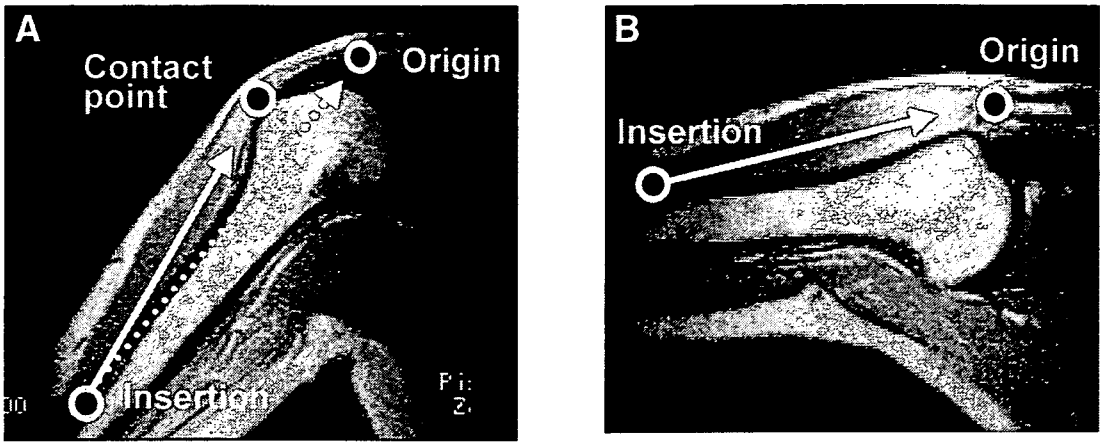

Figure 3 A, In the middle fiber of deltoid, the straight-line vector from the insertion point to the origin point penetrates the bone (*dotted arrow*) at 60° abduction and below; therefore, the muscle vector is established from the insertion point to the contact point (*solid arrow*). **B**, The muscle vector is determined from the insertion point to the origin point over 60° abduction (*arrow*).

langen, Germany) with the arm positioned in 30°, 60°, 90°, 120°, and 150° abduction in a scapular plane. A T_2-weighted, 2-dimensional gradient-echo sequence was applied (repitition time [TR], 304.0 milliseconds; echo time [TE], 25.9 milliseconds; flip angle, 60°; field of view [FOV], 220 mm^2; matrix, 192 × 256; slice thickness, 5 mm). On the image representing the midportion of the middle fiber of the deltoid, a straight line connecting the insertion and the origin was drawn by use of Analyze 3.0 software (Biomechanical Imaging Resource). The slice in which the straight line penetrated the humerus was then studied. As a result, the straight line penetrated the humerus at 60° abduction and below in 8 of 10 subjects, including the volunteer who provided the CT data.

From this result, the muscle vector of the middle fiber of the deltoid was established from the insertion to the contact point at 60° abduction and below and from the insertion to the origin over 60° abduction. Finally, the musculoskeletal model was obtained as shown in Figure 4. A triangular shape demonstrates the muscle with a wide origin area (F1-F6).

The analyzed motion was abduction of the shoulder joint in the scapular plane ranging from 10° to 150°. During abduction, the shoulder joint was kept in neutral rotation, the elbow joint in full extension, and the forearm in neutral rotation. In this model, not only glenohumeral joint motion but also scapulothoracic motion was considered. Motion of the scapula was reproduced according to a previous in vivo study,[9] and all of the coordinate points on the scapula and upper arm were transformed as the position of the scapula changed. The glenohumeral joint was defined as a ball joint, and the center of the humeral head, which was approximated to a sphere, was defined as the center of rotation. The upper extremity was assumed to be a rigid body. The self-weight of the upper extremity, which was defined to be 5.2% of the body weight,[13] was applied at the middle point between the shoulder and wrist joint. The self-weight was considered to be the only external force in this analysis. Internal forces acting on the upper extremity were the muscle forces and the joint reaction force. No

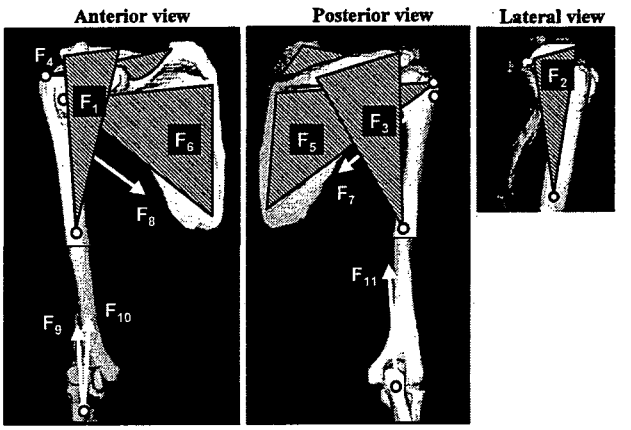

Figure 4 Musculoskeletal model. The triangular shape represents a wide muscle (F1-F6). *F1*, Anterior fiber of deltoid; *F2*, middle fiber of deltoid; *F3*, posterior fiber of deltoid; *F4*, supraspinatus; *F5*, infraspinatus; *F6*, subscapularis; *F7*, teres minor; *F8*, teres major; *F9*, long head of biceps; *F10*, short head of biceps; *F11*, long head of triceps.

friction at the articular surface was considered. Because the muscle forces and joint reaction force were obtained only from the equilibrium equations of force in this study, any ligaments or capsules that demonstrated no force were not considered.

Three-dimensional static equilibriums on force and moment were formulated by use of force vectors as shown in Figure 5, where F_i indicates the magnitude of the muscle forces, $\vec{W}$ represents the gravity vector of the self-weight of the upper extremity, and $\vec{R}$ represents the reaction force vector. By denoting the unit vector of the muscle forces by $\vec{u}_i$, and the position vector of the action points of the muscle forces, the reaction force, and the self-weight by $\vec{r}_i$, $\vec{r}_r$, and $\vec{r}_w$, respectively, the equilibrium equations on force and moment can be expressed as Equations 1 and 2:

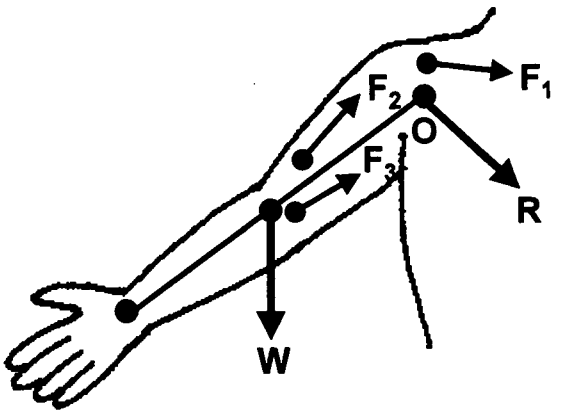

Figure 5 Three-dimensional biomechanical model for formulation. F_i, Each muscle force (i = 1-11); R, joint reaction force; W, self-weight of upper extremity.

$$\sum_{i=1}^{11} F_i\vec{u}_i + \vec{R} + \vec{W} = 0 \quad (1)$$

$$\sum_{i=1}^{11} (\vec{r}_i \times F_i\vec{u}_i) + \vec{r}_r \times \vec{R} + \vec{r}_w \times \vec{W} = 0 \quad (2)$$

Because a value of muscle force must not be negative, the following expression can be indicated:

$$F_i \geq 0 \quad (3)$$

Six equations derived from Equations 1 and 2 along each of the x-, y-, and z-axes have 14 unknown quantities, which are 11 muscle forces and 3 components of the joint reaction force. This equation system indicates an indeterminate problem with an infinite number of solutions. To find a unique solution, an optimization technique by the successive quadratic programming method was applied. An objective function used in the successive quadratic programming method is defined as the total sum of the square of the muscle stress, which is the muscle force divided by the physiologic cross-sectional area (PCSA), and is expressed as Equation 4:

$$U = \sum_{i=1}^{11} (F_i/PCSA_i)^2 \quad (4)$$

The value of PCSA of each muscle was obtained from a previous study[10] (Table I). The objective function U was minimized by use of Equation 1, Equation 2, and inequality (Equation 3) as the constrained conditions. The optimal origin points of the muscles with a wide origin area were also determined to minimize the objective function at this stage. The static numerical analysis was performed every 5°.

EMG

To validate the results of the computer simulation, we carried out EMG in the same volunteer whose CT data were used to build the musculoskeletal model. The 6-channel Polygraph 360 System (NEC Medical Systems, Tokyo, Japan) was applied for the measurement. Platinum fine-wire electrodes with a diameter of 0.05 mm were used for the supraspinatus, infraspinatus, subscapularis, and teres minor; disposable surface electrodes were used for each fiber of the deltoid, biceps, and triceps. The surface electrodes were attached to the skin over the muscle belly with an inter-electrode center-to-center distance of 30 mm. Abduction movement in the scapular plane from 10° to 150° was statically measured every 10°. The subject was told to stand and hold his upper limb in an abducted position with no extra load for 5 seconds. The position of each joint was matched with the corresponding position of the model. A 1-minute rest period was permitted before changing positions. The data were recorded on a computer by use of Biocorder software (KISSEI COMTEC, Nagano, Japan). For data analysis, the middle 3 seconds of each measurement were selected and integrated by use of BIMUTAS II software (KISSEI COMTEC). The same procedure was repeated 3 times, and the mean value was calculated.

Table 1 PCSA of the analyzed muscles[10]

Muscle	PCSA (cm^2)
F1; Anterior fiber of deltoid	4.5
F2; Middle fiber of deltoid	13.5
F3; Posterior fiber of deltoid	3.9
F4; Supraspinatus	4.5
F5; Infraspinatus	5.8
F6; Subscapularis	9.7
F7; Teres minor	2.6
F8; Teres major	5.8
F9; Long head of biceps	1.9
F10; Short head of biceps	1.3
F11; Triceps	3.9

PCSA, physiologic cross-sectional area

Statistical analysis

To evaluate the correlation between the integrated EMG values and the analyzed muscle forces statistically, a simple regression analysis was performed in each muscle. The muscle force of the biceps was calculated as the sum of the forces of both the long and short heads. The regression functions were considered significant at $P < .05$.

RESULTS

The results of the computer simulation are shown in Figure 6. The muscle forces and the reaction force were normalized and expressed as a percentage of body weight. The middle fiber of the deltoid demonstrated the largest force, with a peak value (27.5% of body weight) at 75° abduction, followed by the supraspinatus (10.9% of body weight), the anterior fiber of the deltoid (9.5% of body weight), and the infraspinatus (8.0% of body weight). These muscles acted continuously during the whole motion. On the other hand, the teres minor was active in the latter half of abduction, and the subscapularis acted only in the

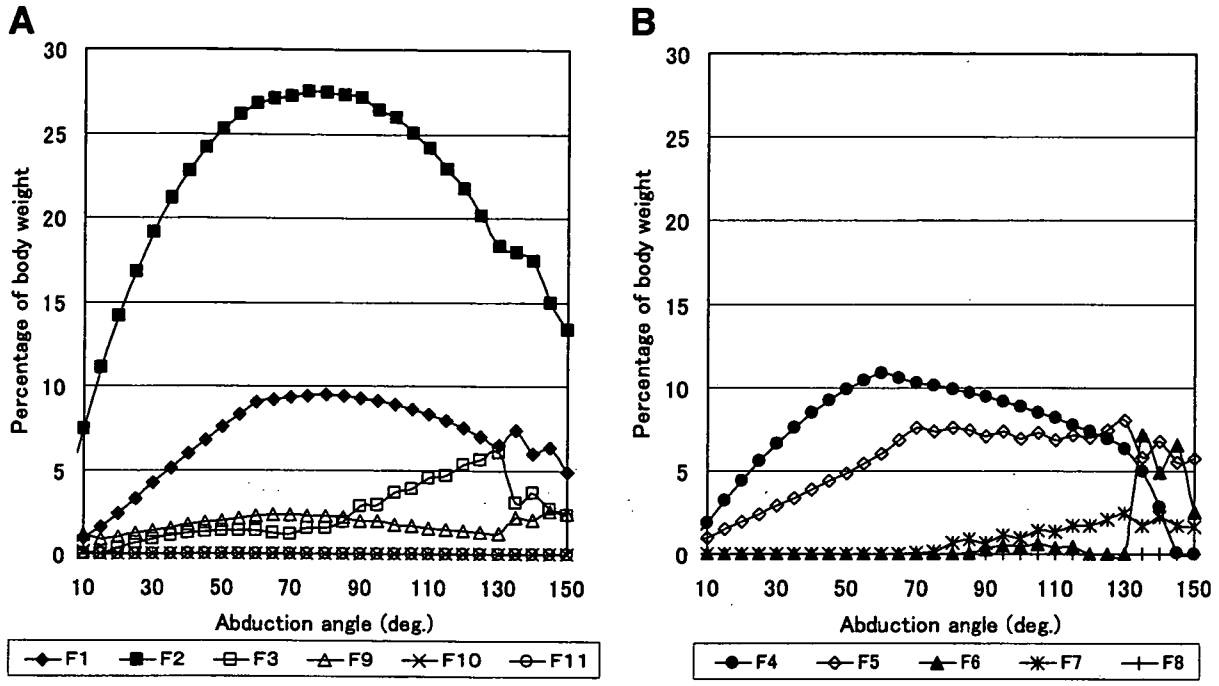

Figure 6 A and **B**, Relationship between muscle force and abduction angle obtained from computer simulation.

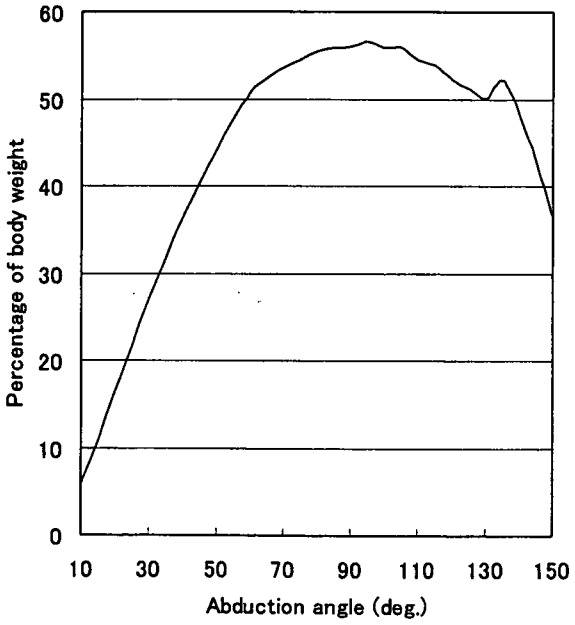

Figure 7 Joint reaction force calculated from method.

last phase. The teres major and triceps demonstrated no muscle forces. The joint reaction force showed its maximum value of 56.5% of body weight at 95° abduction (Figure 7).

The optimal origin points of the 6 wide muscles (F1-F6) selected in each abduction angle changed as the shoulder joint abducted, as shown in Figure 8, which shows the relationship between the optimal point and the abduction angle in the supraspinatus and infraspinatus as examples.

The results of EMG are shown in Figure 9. The middle fiber of the deltoid demonstrated the largest value, followed by the supraspinatus, anterior fiber of the deltoid, and infraspinatus. These muscles showed gradual increases, whereas the analyzed forces peaked and then declined. In the subscapularis, on the other hand, the value increased in the last phase of abduction, as did the analyzed force.

The significant regression functions between the analyzed muscle forces and the integrated EMG values were obtained in all muscles except for the triceps and teres major, which showed no muscle forces in the analysis (Table II).

DISCUSSION

In numerical muscle force analyses, a straight-line vector, a centroid line, or a bony contour line have been mainly used in muscle modeling.[1,4,5,7,11,16,17] However, modeling of a muscle originating from a wide area has been a problem, because it is unreasonable for a single fixed straight-line vector to represent the muscle and, moreover, the direction of the muscle action can change depending on the joint position. To solve this problem, Högfors et al[4] proposed dividing muscles with large attachment sites

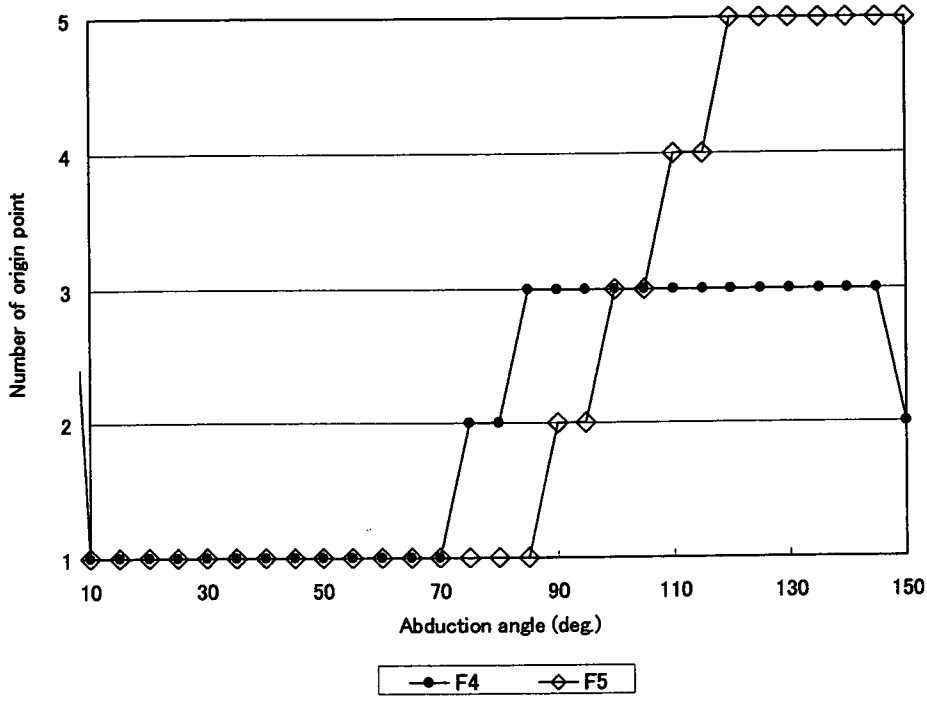

Figure 8 The optimal origin points of the supraspinatus and infraspinatus selected in each abduction angle are indicated as an example.

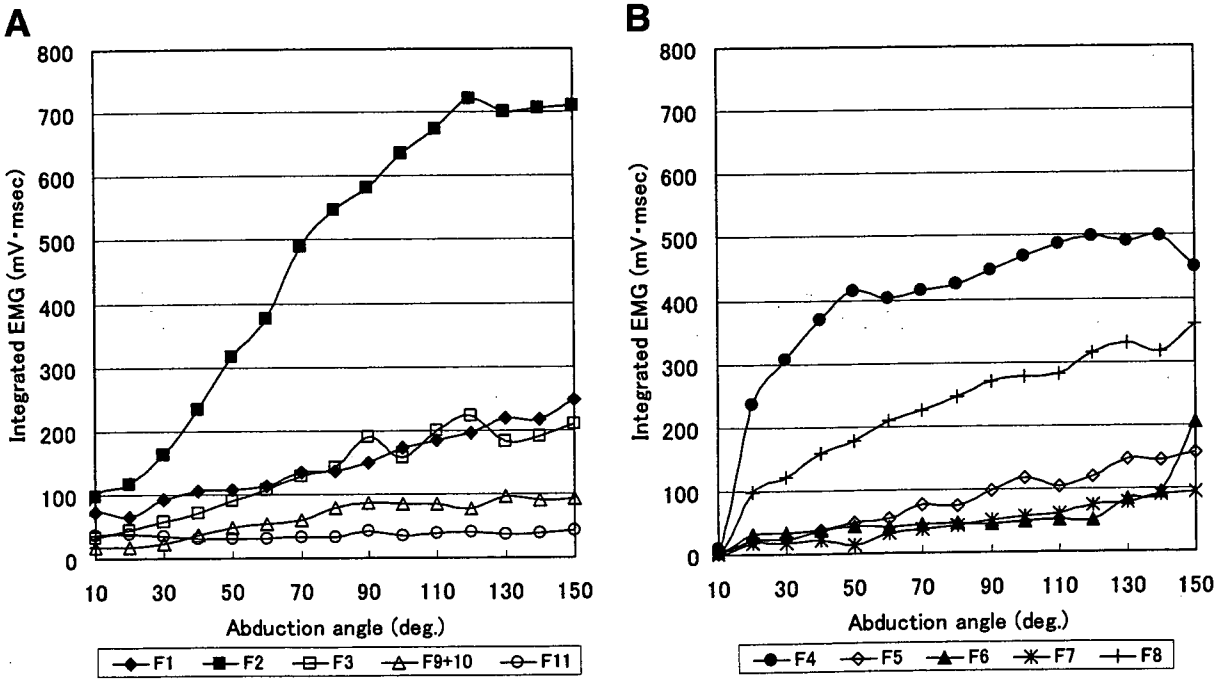

Figure 9 A and **B**, Integrated EMG values.

into several muscle lines of action. Karlsson and Peterson[7] calculated the shoulder muscle forces using the divided vector model and reported that some of the results were reasonable whereas others were not. How to determine the number of muscle lines of action is still controversial, although Van der Helm and

Table 2 The regression functions between the analyzed muscle forces and the integrated EMG values

Muscle	Regression function	P value	R
F1; Anterior fiber of deltoid	y = 57.94 x + 73.49	0.037	0.523
F2; Middle fiber of deltoid	y = 84.79 x + 117.26	0.047	0.503
F3; Posterior fiber of deltoid	y = 159.38 x + 58.57	0.000	0.848
F4; Supraspinatus	y = 111.72 x + 231.86	0.037	0.525
F5; Infraspinatus	y = 85.99 x − 9.96	0.000	0.805
F6; Subscapularis	y = 110.60 x + 44.22	0.010	0.624
F7; Teres minor	y = 158.65 x + 21.52	0.000	0.930
F8; Teres major	unanalyzable		
F9 + F10; Biceps	y = 142.58 x + 14.02	0.048	0.500
F11; Triceps	unanalyzable		

EMG, electromyography

Veenbaas[16] reported that there is an appropriate number of muscle lines that represent a muscle force. In our study, we proposed a new method to determine the optimal origin point of muscles that originate from a wide area; the origin point was not predetermined but was defined in every joint position. The fact that the optimal origin point in each abduction angle shifted in all wide muscles in our study suggests that it is unreasonable for a fixed-line vector to represent these muscles at different moments of a motion. However, as the current model is preliminary, there are some aspects that should be considered for further development of the model. For the muscles in which not only the origin area but also the insertion area is wide, as in the serratus anterior, we also have to consider other options such as dividing the muscles into several parts. The optimal origin point was selected from only several points on the straight line in this study. In the next stage, the optimal point should be picked from any point on the 3-dimensional origin surface.

EMG has been used to validate the results of the analysis by comparing them qualitatively in previous studies.[1,7] However, it is known that EMG amplitude is length-dependent,[3,17] so EMG values cannot be directly compared among different muscles and often result in large amplitudes near full elevation angles, whereas the analyzed forces decrease. In this study, EMG values showed gradual increase, whereas analyzed values showed their peaks at the middle phase of the motion in some of the muscles. Despite that, the muscle forces and EMG values showed quantitative correlations. Therefore, although it is controversial to use EMG values as an indicator for validation because the EMG-force relationship is unknown for shoulder muscles,[17] as long as there is no other established method by which to validate the predicted muscle forces, we consider that EMG can be an indicator to validate (at least) the pattern of muscle forces.

In our study, the maximum joint reaction force was calculated to be 56.5% of body weight. In previous reports, the joint reaction force ranged from 44% to 92% of body weight.[6,7,12,13] Although the values cannot be compared directly because the method, condition, and assumption of each study vary greatly, our result is considered to be a comparable and reasonable value.

There are still some considerable limitations in this study. The model includes only the muscles that originate from the scapula. To simulate various conditions of a shoulder joint, a whole system including bone structures and muscles related to the thorax must be developed. This study is a static analysis with only the equilibrium conditions of force and moment. Therefore, the stiffness and time-dependent fatigue of muscles are not considered, nor are soft tissues such as joint capsules or ligaments that stabilize the glenohumeral joint.

Our model is capable of being applied to individual clinical patients to simulate their shoulder muscle activities, because anatomic data can be easily introduced from CT data. The simulation would provide useful information regarding how the other normal muscles work in a compensatory manner in pathologic conditions, such as tendon ruptures or muscle paralyses. It would also be possible to simulate surgical treatment, such as tendon or muscle transfers, to predict preoperatively the effects of surgical procedures and their influence on the other muscles.

In conclusion, we have developed a 3-dimensional shoulder biomechanical model using an original method of determining vectors of muscles originating from a wide area. The results of the numerical analysis were in correlation with the integrated EMG values, therefore allowing for the simulation of cooperative abduction muscle activities in vivo. We believe that this novel concept will provide a new approach in modeling a variety of muscles with a wide origin area and the possibility for more precise simulations of muscle activities in a living body.

We thank Dr Satoshi Yoshinari, Hokkaido Industrial Research Institute, for his previous work and help, as well as

the radiologic technologists at Sapporo Hokuyu Hospital for their help in collecting the CT data for this study.

REFERENCES

1. Crowninshield RD, Brand R. A physiologically based criterion of muscle force prediction in locomotion. J Biomech 1981;11:793-801.
2. Fujisawa H, Suenaga N, Minami A. Electromyographic study during isometric exercise of the shoulder in head-out water immersion. J Shoulder Elbow Surg 1998;7:491-4.
3. Heckathorne CW, Childress DS. Relationships of the surface electromyogram to the force, length, velocity, and contraction rate of the cineplastic human biceps. Am J Phys Med 1981;60:1-19.
4. Högfors C, Sigholm G, Herberts P. Biomechanical model of the human shoulder—I. Elements. J Biomech 1987;20:157-66.
5. Högfors C, Karlsson D, Peterson B. Structure and internal consistency of a shoulder model. J Biomech 1995;28:767-77.
6. Inman VT, Saunders JB, Abbott LC. Observations on the function of the shoulder joint. J Bone Joint Surg 1944;26:1-30.
7. Karlsson D, Peterson B. Towards a model for force predictions in the human shoulder. J Biomech 1992;25:189-99.
8. Kronberg M, Németh G, Broström LA. Muscle activity and coordination in the normal shoulder. An electromyographic study. Clin Orthop 1990:76-85.
9. McClure PW, Michener LA, Sennett BJ, Karduna AR. Direct 3-dimensional measurement of scapular kinematics during dynamic movements in vivo. J Shoulder Elbow Surg 2001;10:269-77.
10. Meek SG, Wood JE, Jacobsen SC. Model-based, multi-muscle EMG control of upper-extremity prostheses. In: Winters JM, Woo SL-Y, editors. Multiple muscle systems: biomechanics and movement organization. New York: Springer-Verlag; 1990. p. 360-76.
11. Niemi J, Nieminen H, Takala EP, Viikari-Juntura E. A static shoulder model based on a time-dependent criterion for load sharing between synergistic muscles. J Biomech 1996;29:451-60.
12. Parsons IM, Apreleva M, Fu FH, Woo SL. The effect of rotator cuff tears on reaction forces at the glenohumeral joint. J Orthop Res 2002;20:439-46.
13. Poppen NK, Walker PS. Forces at the glenohumeral joint in abduction. Clin Orthop 1978:165-70.
14. Sigholm G, Herberts P, Almström C, Kadefors R. Electromyographic analysis of shoulder muscle load. J Orthop Res 1984;1:379-86.
15. Suenaga N, Minami A, Fujisawa H. Electromyographic analysis of internal rotational motion of the shoulder in various arm positions. J Shoulder Elbow Surg 2003;12:501-5.
16. Van der Helm FCT, Veenbaas R. Modelling the mechanical effect of muscles with large attachment sites: application to the shoulder mechanism. J Biomech 1991;24:1151-63.
17. van der Helm FCT. Analysis of the kinematic and dynamic behavior of the shoulder mechanism. J Biomech 1994;27:527-50.

Massive rotator cuff tears repaired on top of humeral head by McLaughlin's procedure

Naomi Oizumi, MD,[a] Naoki Suenaga, MD,[a] Kimitaka Fukuda, MD,[b] and Akio Minami, MD,[a]
Sapporo and Mikasa, Japan

The clinical and radiographic outcomes of McLaughlin's procedure for massive rotator cuff tears were investigated in 25 shoulders, in which the cuff tears were so severe that the tendons were sutured on the top of the humeral head. The mean age at surgery was 62.2 years (range, 39-74 years). The mean follow-up period was 50 months (range, 24-80 months). The University of California, Los Angeles score significantly improved from 10.9 to 31.8 points postoperatively; the postoperative result was classified as excellent in 11 shoulders, good in 11, and poor in 3. Osteoarthritis progressed postoperatively in 7 shoulders (28%), and upper migration of the humeral head progressed in 6 (24%), although both progression rates were no higher than those for other common procedures. When torn tendons reach over the top of the humeral head with the arm at the side in patients with massive tears that are not reparable to the greater tuberosity, satisfactory clinical outcomes can be expected. (J Shoulder Elbow Surg 2007;16:321-326.)

Although various surgical procedures have been reported for massive rotator cuff tears,[1-16,18] McLaughlin's procedure has provided the most stable results[2,4,6,9-11,14,18] and has been considered as the first choice. A number of chronic massive tears could be repaired by McLaughlin's procedure after sufficient intraarticular and extraarticular mobilization techniques. It is often impossible to repair the torn tendon edge at the original site without excessive tension in severe cases, and medialization of the reinsertion of the tendon onto the articular surface of the humeral head is indicated.[10,14] However, if the reinsertion is medialized excessively, there will be some potential risks as follows: severe restrictions of the movement of the glenohumeral joint, loss of normal shoulder function as a result of the change in the kinematics, and damage to the articular cartilage of the humeral head, which may lead to the osteoarthritis (OA) of the glenohumeral joint. Therefore, it is important to establish the acceptable extent of the medialization. Liu et al[8] reported a cadaveric study to determine to what extent the cuff tendon could be advanced medially. However, no clinical study has evaluated the results of medialization of the cuff tendon for massive rotator cuff tears, clearly focusing on the extent of the medialization.

In all of the cases in this study, the cuff tears were so severe that the bone troughs for the tendon repair needed to be made on the top of the humeral head. The objectives of this study are to evaluate the clinical and radiographic outcomes in patients with medialization of the reinsertion for severe massive cuff tears and to investigate the limitations of this procedure.

MATERIALS AND METHODS

We evaluated 25 shoulders in 25 patients with severe, massive rotator cuff tears treated by McLaughlin's procedure from 1994 to 1999 with medialization of the reinsertion of the cuff tendon on the top of the humeral head for this study. The bone troughs for the repair were made just on the lateral side of the apex of the humeral head because the tendon could not reach farther with the arm at the side in all cases. The top of the humeral head was determined intraoperatively with the arm at the side and the shoulder in a neutral position, and the location of the bone trough was defined as follows: when the distance between the top of the humeral head and the greater tuberosity is equally divided into 3 sections, the bone trough was made in the section nearest the top of the humeral head (Figure 1). The cases in this study comprised 10% of all cases of tendon-to-bone repair procedures performed for rotator cuff tears during the same period. All 25 patients were investigated by direct physical examination and radiographic examination more than 2 years after surgery. There were 15 men and 10 women, and the operative shoulder was the right in 21 and the left in 4. The mean age at the time of surgery was 62.2 years (range, 39 to 74 years). The torn tendons were the supraspinatus and infraspinatus in 22 shoulders; supraspinatus, infraspinatus, and teres minor in 2; and

From the [a]Department of Orthopaedic Surgery, Hokkaido University School of Medicine, Sapporo, and [b]Department of Orthopaedic Surgery, Mikasa City General Hospital, Mikasa.

Reprint requests: Naomi Oizumi, MD, Department of Orthopaedic Surgery, Hokkaido University Graduate School of Medicine, Kita-15, Nishi-7, Kita-ku, Sapporo, 060-8638, Japan (E-mail: nao9877@aol.com).

1058-2746/2007/$32.00
doi:10.1016/j.jse.2006.08.004